Stabilizing and increasing the magnetic moment of half-metals: The role of Li in half-Heusler LiMnZ (Z=N, P, Si)

L. Damewood,[1,*] B. Busemeyer,[2] M. Shaughnessy,[3] C. Y. Fong,[1] L. H. Yang,[4] and C. Felser[5]

[1]*Department of Physics, University of California, Davis, California 95616, USA*

[2]*Department of Physics, University of Illinois at Urbana-Champaign, Urbana, Illinois 61801, USA*

[3]*RTBiQ, Inc., San Francisco, California 94121, USA*

[4]*Lawrence Livermore National Laboratory, Livermore, California 94551, USA*

[5]*Institut für Anorganische Chemie und Analytische Chemie, Johannes Gutenberg-Universität Mainz, 55099 Mainz, Germany*

(Received 18 March 2012; revised manuscript received 20 January 2015; published 6 February 2015; publisher error corrected 27 February 2015)

Due to their similarities to metastable zinc-blende half-metals, we systematically examined the half-Heusler compounds β-LiMnZ (Z = N, P and Si) for their electronic, magnetic, and stability properties at optimized lattice constants and strained lattice constants that exhibit half-metallic properties. We also report the other phases of the half-Heusler structure (α and γ phases), but they are unlikely to be grown. The magnetic moments of these stable Li-based compounds are expected to reach as high as $4\mu_B$ per unit cell when Z = Si and $5\mu_B$ per unit cell when Z = N and P; however, the antiferromagnetic spin configuration is energetically favored when Z is a pnictogen. β-LiMnSi at a lattice constant 14% larger than its equilibrium lattice constant is a promising half-metal due to its large magnetic moment, large gap, and vibrational stability. The modified Slater-Pauling rule for these compounds is determined. Finally, we investigated a plausible method for developing half-metallic Li$_x$MnZ at equilibrium by tuning x, but this type of alloying introduces local structural changes that preclude half-metallicity.

DOI: 10.1103/PhysRevB.91.064409 PACS number(s): 75.50.−y, 85.75.−d, 75.50.Pp

I. INTRODUCTION

Ternary compounds involving the Li atom in the form of half-Heusler, or semi-Heusler, alloys have recently attracted attention because of their potential in optoelectronic and spintronic applications [1–3]. The crystal structure, $C1_b$, of any half-Heusler alloy is similar to the structure, $L2_1$, of a full-Heusler alloy (X_2YZ) but missing one X. Due to the missing element, these alloys have three distinct atomic arrangements, called α, β, and γ phases [4], used by various research groups [1,2,4–8]. In Table I, the positions occupied by the three atoms and the vacancy are given according to the notations defined by Wyckoff [9]. The alternative notation of Roy *et al.* [3], in which the element that is tetrahedrally coordinated with the other two is underlined, is provided in the last column for comparison. Kieven *et al.* [1] examined lithiated half-Heusler alloys in the β phase, namely, LiMgZ (Z = N, P, As, Bi), LiYP, LiYP (Y = Zn, Cd), and LiAlSi. They found that covalent bonding between the Y and Z atoms forms the gap of these compounds. They suggested that these half-Heusler alloys could be used in optoelectronic and solar applications because the values of the band gaps and lattice constants of these materials are suitable for substituting CdS as buffer layer materials. Recently, Roy *et al.* [3] considered 987 potential half-Heusler alloy configurations for their piezoelectric properties. Since there were no magnetic elements in any of the alloys, the magnetic properties were not addressed. Jungwirth *et al.* [2] considered a magnetic element in a Li-based half-Heusler alloy and epitaxially grew β-LiMnAs on an InAs substrate. They predicted that β-LiMnAs is antiferromagnetic and confirmed it experimentally using a superconducting quantum interference device (SQUID) to measure the magnetic moment.

Studies of transition-metal-element (TME) based half-Heusler alloys indicate that there are a number of differences among the three half-Heusler phases. Using the α phase for TME-based half-Heusler alloys, Tobola and Pierre [8] and Galanakis *et al.* [7] showed that the d-d bonding between X and Y of the half-metal (HM) CrMnSb is responsible for the small gap in the insulating channel. A HM exhibits metallic properties in one spin channel and semiconducting properties in the oppositely oriented spin channel. They did not comment on the d-p bonding states between X and Z. We previously suggested [10] a point of view in Heusler alloys unifying the d-p and the d-d bonding: Z is the most electronegative among the three atoms, so it should form d-p bonding and determine the primary properties of the bonding-antibonding gap. The weak bonds between the two TM atoms, formed by d-d bonding, contribute to the states at the gap and result in a much smaller gap. From this point of view, the TME-based half-Heusler alloys, such as CrMnSb in α and γ phases, differ by which of the two TM atoms is the nearest neighbor (nn) of Z. Their properties differ accordingly.

How does our suggestion to consider the nn of Z work for Li-related half-Heusler alloys? We expect that the β phase is energetically favored because Z, the most electronegative element, is the nn to both Li and Mn. We also anticipate a larger gap than in the TME-based half-Heusler alloys since there is no d-d bonding forming states in the gap. Based on the fact that Li easily gives up its outermost electron to its neighbor, β-LiMnZ can be viewed as an intercalation of zinc-blende $(\mathrm{Mn}Z)^-$ and Li^+ [1]. According to the ionic model [11], Mn loses three valence electrons to the pnictogen Z when they are nn pairs, and the four remaining d electrons combine with the

*damewood@physics.ucdavis.edu

TABLE I. The positions of the three atoms, X, Y, and Z, in terms of the Wyckoff notation: 4a = (0, 0, 0)a, 4b = (1/2, 1/2, 1/2)a, and 4c = (1/4, 1/4, 1/4)a, where a is the lattice parameter. The zinc-blende structure, YZ, is included for comparison. The last column shows the alternative notation by Roy *et al.* [3] in which the 4c site is underlined.

Structure	X	Y	Z	Tetrahedral notation [3]
α	4c	4b	4a	$\underline{\text{X}}$YZ
β	4b	4a	4c	X$\underline{\text{Y}}$Z
γ	4a	4c	4b	XY$\underline{\text{Z}}$
Zinc blende		4a	4c	

electron from Li to give a local magnetic moment as large as $5\mu_B$ per Mn. If Z is a group-IV element, then the maximum is $4\mu_B$ per Mn.

Typical TME-based zinc-blende alloys, such as MnZ, are not half-metallic at their equilibrium lattice constant. The standard method to obtain half-metallic properties from these alloys is to increase (shrink) their lattice constant by growing them as thin films on substrates with larger (smaller) lattice constants [12]. Straining the lattice constant of the alloy can manifest half-metallic properties by changing the bonding and exchanging the strength between atoms [13]. These changes can shift the Fermi energy into a gap of one spin channel while the Fermi energy cuts through states in the other spin channel, resulting in a HM. We examine the alloys for large magnetic moments or half-metallic properties at lattice constants away from equilibrium.

Since Li-based alloys, other than the ones included in this paper, may be desirable to grow if their magnetic moments are known *a priori* to be large, we determined the modified Slater-Pauling (SP) rule [14] for Li-based half-Heusler alloys based on the band structure calculations. The rule provides a zeroth-order approximation to the magnetic moment of ferromagnets based on the number of occupied states in the semiconducting spin channel $N_\downarrow$. Combined with the fact that the total number of valence states is $N = N_\downarrow + N_\uparrow$, the magnetic moment is

$$\begin{aligned} M &= N_\downarrow - N_\uparrow \\ &= N - 2N_\downarrow \end{aligned} \quad (1)$$

in units of μ_B. The modified SP rule is useful for predicting the magnetic moment of materials where $N_\downarrow$ may remain constant, but N changes by replacing atoms with neighboring atoms on the periodic table. As mentioned previously, Jungwirth *et al.* [2] already determined that β-LiMnAs favors the antiferromagnetic configuration, so we examined the possibility that ferromagnetism is energetically favored over antiferromagnetism in any of the alloys.

With the Li-based alloys, it seems plausible to shift the Fermi energy E_F by adjusting the concentration of Li atoms. For an alloy whose E_F cuts through the bottom of the conduction band of one spin channel, will lowering the concentration of Li push the Fermi energy into the gap and give a HM at equilibrium? We use the location of E_F with respect to the gap as a guide to investigate the possibility of half-metallicity in the $Li_{0.75}$MnP alloy.

For these alloys to be useful in devices, the issue of stability should be addressed. In the past, the conventional wisdom was that the thin-film forms of HMs with lattice constants away from the equilibrium values are stable up to about 100 layers [12], but we question this claim. We compared the stability of β-LiMnP to metastable zinc-blende (ZB) MnP, by considering the phonon band structure determined by the response-function method [15].

In this paper, we investigate three LiMnZ, with Z = N, P, and Si, and address the following issues:

(i) What are the basic bonding and magnetic properties of LiMnZ, particularly in the lowest-energy phase?

(ii) Compared to zinc-blende MnZ, what is the role of Li in the electronic and magnetic properties of LiMnZ?

(iii) Can any of the alloys energetically favor the ferromagnetic phase and give a large magnetic moment? What is the modified SP rule for these alloys?

(iv) Can adjusting the concentration of Li in β-LiMnZ result in a HM at equilibrium?

(v) How does the phonon stability of β-LiMnZ compare to ZB MnZ, and what are the implications for growth?

In Sec. II, we discuss the models used to answer these questions and present a brief description of the methods of calculation. Results and discussion of the above issues will be presented in Sec. III. Finally, in Sec. IV, we summarize our findings.

II. STRUCTURAL MODELS AND METHODS OF CALCULATION

We used the primitive cell to find the equilibrium lattice constants by means of minimizing the total energy of each alloy with respect to the lattice constant. The phonon calculations also rely on the respective primitive cells of β-LiMnP and ZB MnP. We calculate the antiferromagnetic properties by constructing a tetragonal cell consisting of 2 f.u. of LiMnZ to allow the possibility of antiparallel alignment of Mn atoms. Additionally, we explored the possibility of lower concentrations of Li atoms by constructing conventional unit cells consisting of 4 f.u. of LiMnZ and then removing one or more Li atoms and letting the ions and unit cell relax to equilibrium. The resulting alloys are denoted $Li_xMn_4Z_4$, where x = 1, 2, or 3, or Li_yMnZ, where y = 0.25, 0.50, 0.75.

We used the spin-polarized version of the VASP code [16–19], which is based on density functional theory (DFT) [20]. The generalized gradient approximation (GGA) of Perdew, Burke, and Ernzerhof (PBE) [21] was used to treat the exchange correlation between electrons. GGA provides realistic bonding and magnetic properties, except for the value of the semiconducting gap. The value of the semiconducting gap is not a crucial issue at this point, so we did not consider more complicated methods utilizing many-body techniques or hybrid functionals. Many-body methods improve upon the conduction states in HMs [22] but also show that half-metallic properties may disappear at finite temperatures [23].

The VASP package provides projector-augmented-wave (PAW) pseudopotentials [24] for Li, Mn, N, P, and Si that were constructed using PBE. We used a basis of plane waves with a 1000 eV kinetic energy cutoff for all calculations. The Monkhorst-Pack [25] meshes of (17,17,17), (15,15,15), and (11,11,11) were adopted for the Brillouin zone (BZ) of the primitive, tetragonal, and the conventional cells, respectively.

Using these values, the convergence of the total energy and the magnetic moment of any sample are better than 1.0 meV and 1.0mμ_B, respectively.

To address the stability of the lithiated compounds, we used the ABINIT software package to perform response-function phonon calculations [26,27]. We used the same exchange-correlation functional as in VASP and used comparable convergence parameters to calculate the ground-state structure. To calculate the force constants, a $4 \times 4 \times 4$ irreducible $\vec{q}$-point grid, centered at $\vec{q} = (0,0,0)$, was constructed.

III. RESULTS AND DISCUSSION

A. Bonding properties of LiMnZ

Using the primitive unit cell, we first determined the equilibrium lattice constants of the three compounds in the three phases (α, β, and γ phases). The results are summarized in Table II. The lattice constants correlate with the covalent radii of Z (0.71, 1.09, and 1.14 Å for N, P, and Si, respectively [28]). The β phase is consistently the lowest-energy phase because Z, the most electronegative element, is the nn to both Mn and Li.

In Fig. 1, we show the density of states (DOS) for α- and β-LiMnSi with the partial DOS of the so-called e_g (doubly degenerate d_{z^2} and $d_{x^2-y^2}$) and t_{2g} (triply degenerate d_{xy}, d_{yz}, and d_{zx}) states. Here, we choose to discuss the bonding properties of LiMnSi since, at the equilibrium lattice constant, the overall bonding features are not significantly altered when $Z =$ N or P. The β- and γ-phase DOSs are very similar: both have Mn and Si as the nn, and the position of the Li atom does not drastically alter the DOS, so the γ-phase is not included. The β and γ phases form a large bonding-antibonding gap due to the overlap of the t_{2g} states of Mn and Si sp^3 states in the tetrahedral environment. The α phase is significantly different from the β and γ phases and does not form a large bonding-antibonding gap because Mn and Si are second neighbors in a cubic environment.

B. The role of Li in LiMnZ

We have argued that Li easily gives up its valence electron to its nearest neighbor. To substantiate this argument, we compare β-LiMnSi to MnSi in the ZB structure. The latter is predicted

TABLE II. The equilibrium lattice constants, total energies, and magnetic moments for three lithiated half-Heusler alloys.

Compound	Lattice constant (Å)	Total energy relative to β (eV)	Magnetic moment (μ_B/Mn)
α-LiMnN	4.961	2.379	4.675
β-LiMnN	4.912	0.000	3.925
γ-LiMnN	5.139	1.992	4.805
α-LiMnP	5.600	1.218	4.391
β-LiMnP	5.717	0.000	4.090
γ-LiMnP	5.715	0.661	3.987
α-LiMnSi	5.629	0.721	3.750
β-LiMnSi	5.778	0.000	3.314
γ-LiMnSi	5.788	0.395	3.301

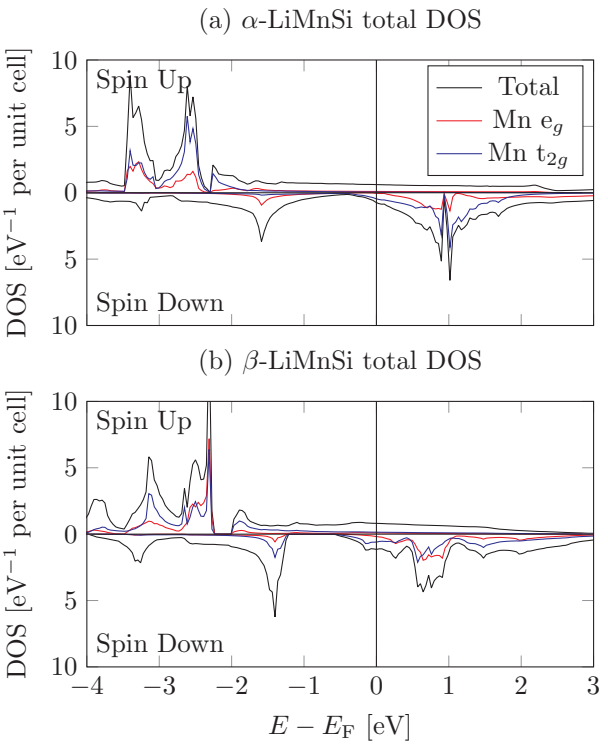

FIG. 1. (Color online) Spin-polarized total density of states (DOS) for LiMnSi in (a) α and (b) β phases at their respective equilibrium lattice constants. The Mn e_g and t_{2g} partial DOS are shown as red and blue lines, respectively.

to be a HM in which the bonding, antibonding, and nonbonding states are easily identified [13]. In Fig. 2, we compare the states around E_F at Γ of the two spin channels for β-LiMnSi and MnSi at the same lattice constant of 5.778 Å and show the size of the bonding-antibonding gap (the energy difference between the top of the valence band and the bottom of the conduction band in the minority spin channel at the Γ point). The primary effects of Li are (1) increasing the width of the occupied states and (2) promoting its s state to the p states and contributing to the d-p mixed states. The second effect indicates that Li gives up its electron. The argument that the Li is giving up its electron is also reflected in the charge-density difference, β-LiMnSi minus MnP, shown in Fig. 3. This plot shows the Li electron redistributes its charge to Mn [labeled (i)] and Si [labeled (ii)], away from Li, and causes the d-p hybridized bond between Mn and Si to weaken, thereby shifting the bond charge away from Si and towards Mn [labeled (iii)].

The pnictides in the β phase do not have integer magnetic moments and show no gap in either spin channel near E_F. According to our criteria, they are not HMs [29]. Due to the presence of the highly electronegative pnictogen, the Li electron is not completely transferred to the Mn. Instead, the electron from Li causes a reduction in the strength of the d-p hybridization between the pnictogen and the Mn under the tetrahedral environment. With the reduction in the hybridization, the bonding-antibonding gap shrinks, and the bottom of the conduction band in the minority spin channel of β-LiMnZ becomes occupied.

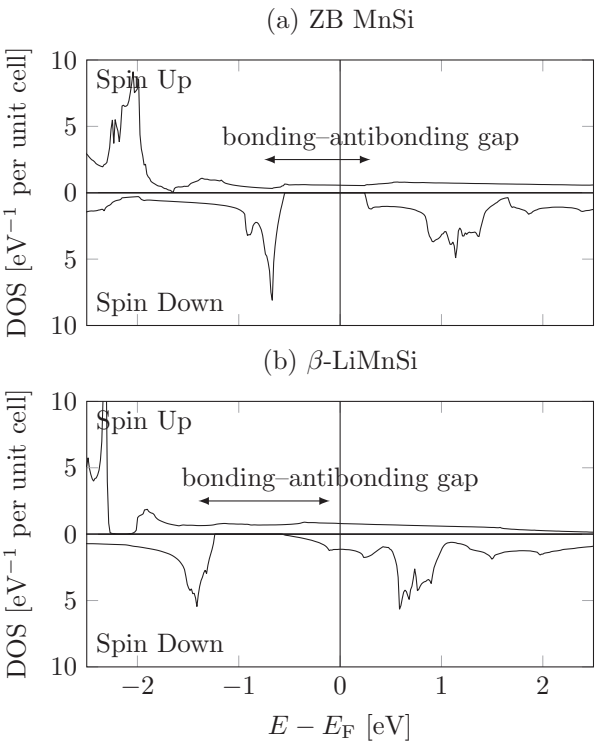

FIG. 2. Density of states for (a) zinc-blende MnSi and (b) β-LiMnSi at the optimized lattice constant. The arrows indicate the size of the bonding-antibonding gap at the Γ point.

C. Magnetic and half-metallic properties

We are interested in adjusting the lattice constant to force the values of the magnetic moments to be as large as possible. In practice, the consensus is that many devices are thin films and can be grown to match the lattice constants on selected substrates. We can use our results to predict the substrates that match the lattice constants of our compounds with large magnetic moments, but we believe that this will not always be possible for large lattice constants or energies far from equilibrium; therefore, the issue of stability will be addressed later. Tetragonalization can also occur during growth, but it will not necessarily destroy half-metallicity [30]. In Table III, we present detailed ferromagnetic properties of the three compounds in the primitive cells of the three types of structures.

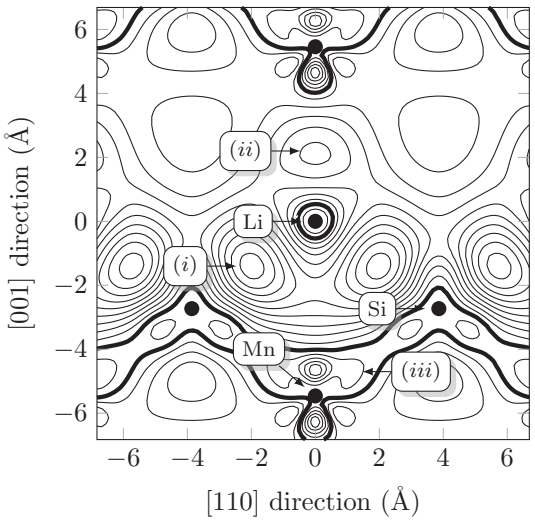

FIG. 3. Contour of the charge-density difference (β-LiMnSi minus ZB MnSi) at the same lattice constant. Circles indicate the location of atoms. Labels (i) and (ii) indicate where the Li electron bonds with Si and Mn, respectively, giving a positive contour. Label (iii) shows the area where the bond between Mn and Si weakens and the contour region is negative. The thick black lines indicate the zero contours.

TABLE III. Summary of the lattice constants, total energies, magnetic moments per unit cell, and energy gaps near the Fermi energy E_F (with spin channel) of the three compounds in the three phases where the magnetic moment is largest or integer.

Compound	Lattice constant (Å)	Total energy relative to equilibrium β (eV)	Magnetic moment (μ_B/Mn)	Energy gap near E_F (eV)
α-LiMnN	5.300	0.274	5.000	0.819 ↓
β-LiMnN	5.641	1.097	4.990	Metal
γ-LiMnN	5.571	2.463	5.000	Metal
α-LiMnP	6.250	0.668	5.000	0.341 ↓
β-LiMnP	6.550	0.944	5.000	1.693 ↓
γ-LiMnP	7.248	3.326	5.000	Metal
α-LiMnSi	6.274	1.384	4.050	Metal
β-LiMnSi	6.250	0.318	4.000	0.915 ↓
γ-LiMnSi	6.300	0.392	4.000	0.723 ↓

In Table III, every alloy with an integer magnetic moment and a gap is a HM. These include α-LiMnN, α-LiMnP, β-LiMnSi, β-LiMnP, and γ-LiMnSi. The lattice constant can be increased slightly without destroying the half-metallicity since there is a range of lattice constants where E_F falls within the gap of the semiconducting channel. The magnetic moments of the HMs agree with the predictions of the ionic model plus the contribution of the Li electron to the moment of Mn. The remaining alloys are ferromagnets, and any change in the lattice constant will decrease the moment. Some of the important features of the individual half-Heusler alloys are discussed below.

In Fig. 4, we show the band structures of β-LiMnSi at two lattice constants: the equilibrium lattice constant and the half-metallic lattice constant. The lowest bands are from the s orbitals of Si. The next bands, shown in Fig. 4, are the so-called t_{2g} triply degenerate states at the Γ point that split into doubly (upper) and singly (lower) degenerate states as $\vec{k}$ moves towards X or L. The next higher-energy states at the Γ point are originally from e_g states of Mn. Since their lobes point away from nn Si and toward the second neighbor (sn) of Mn, they do not strongly interact with any other states, so they are called the nonbonding states. The half-metallic gap in Fig. 4(b) is formed between the e_g states and the doubly degenerate states that split off of the t_{2g} states. Using the band structure, we can understand why this half-Heusler alloy is not a HM at the equilibrium lattice constant. The e_g states are insensitive to the separation between nn, but the smaller equilibrium lattice constant causes E_F to shift up and intersect

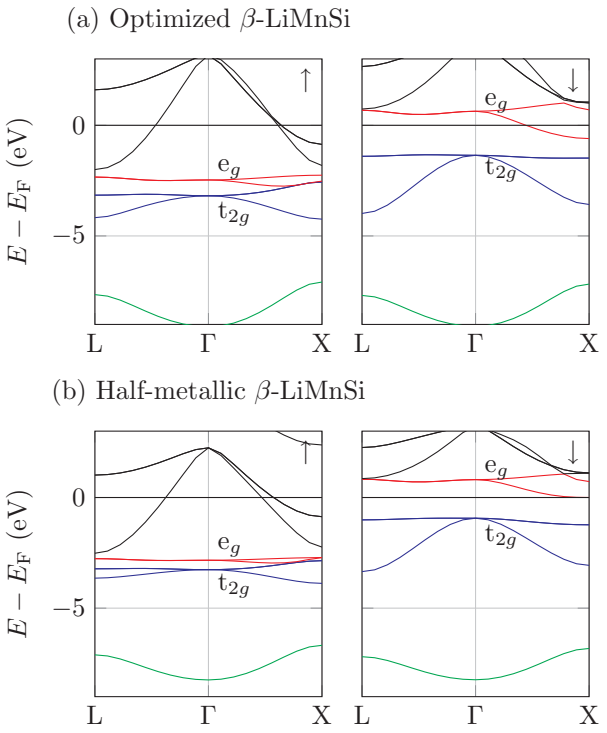

FIG. 4. (Color online) Band structure for β-LiMnSi along L-Γ-X at (a) the equilibrium lattice constant $a = 5.778$ Å and (b) the half-metallic lattice constant $a = 6.250$ Å. The triply degenerate states t_{2g} and the doubly degenerate states e_g near E_F are labeled.

with the e_g states [Fig. 4(a)], resulting in the disappearance of the half-metallicity.

The reason that α-LiMnSi is not a HM can be attributed to the fact that Si forms a nn pair with Li and a sn pair with Mn. The qualitative details are as follows: (i) Ideally, the Li electron can form a covalent bond with Si because the electronegativity of Si is not as large as either P or N. (ii) The sn configuration between Si and Mn favors the p states of Si to form bonds with three Mn electrons. The bonds are not strong enough to form a gap. Consequently, the TM does not completely transfer its three d electrons to Si and gives a moment of $4.050\mu_B$. The pnictides exhibit half-metallic properties in the α phase at lattice constants larger than their respective equilibrium values. The gap for α-LiMnP is 0.376 eV, while it is 0.696 eV for α-LiMnN. The gaps reflect the strength of the electronegativity of P with respect to N and the differing lattice constants. The gaps are formed by the t_{2g} states of Mn and the sp^3 states of the pnictogen, as in the β and γ phases, but with a much smaller bonding-antibonding gap.

Next, we focus on the antiferromagnetic cases. In order to investigate this phase, we use the tetragonal cell so that there are two Mn atoms which can have their magnetic moments oriented oppositely. In Table IV, we present the results for the three half-Heusler alloys in the antiferromagnetic phase and their energy difference with respect to the ferromagnetic half-metallic case. From our calculations, all three phases of LiMnSi can be ferromagnetic HMs, while LiMnN and LiMnP can be antiferromagnetic HMs at the half-metallic lattice constant, much like β-LiMnAs [2].

TABLE IV. Summary of lattice constant and the energy difference between AFM and FM orderings of the three compounds at lattice constants given in Table III. Negative energy differences indicate that the AFM phase is energetically preferred.

Compound	$E_{AFM} - E_{FM}$ relative total energy (eV)
α-$Li_2Mn_2N_2$	−0.037
β-$Li_2Mn_2N_2$	−0.292
γ-$Li_2Mn_2N_2$	−0.302
α-$Li_2Mn_2P_2$	−0.026
β-$Li_2Mn_2P_2$	−0.123
γ-$Li_2Mn_2P_2$	−0.087
α-$Li_2Mn_2Si_2$	+0.100
β-$Li_2Mn_2Si_2$	+0.347
γ-$Li_2Mn_2Si_2$	+0.324

The lithiated half-Heusler alloys have either 13 or 12 valence electrons per unit cell. Since the total number of valence electrons N_t is smaller in these alloys than in the TM-related compounds, a different modified SP rule should be determined. The band structure of β-LiMnSi in the primitive cell, shown in Fig. 4(b), shows four bands in the semiconducting channel, so $N_\downarrow = 4$. From Eq. (1), the new rule is

$$M = (N_t - 8) \tag{2}$$

μ_B per formula unit, so for LiMnSi, $N_t = 12$ and M is $4\mu_B$ per formula unit. Similarly, M is $5\mu_B$ per formula unit for the pnictides. The calculated moments in Table III agree well with the predicted results of Eq. (2); however the modified SP rule is not able to account for the antiferromagnetism in the cases where Z is a pnictogen.

D. Adjusting the Li concentration

Based on the fact that the density of states of some optimized Li-based half-Heusler alloys has E_F above the conduction band edge in the minority spin channel, for example, β-LiMnSi shown in Fig. 2, we decided to find new HMs by adjusting the Li concentration from the conventional cell. The symmetry of the half-Heusler phases allows the removal of any Li atom in the conventional unit cell, and the resultant sample is labeled β-$Li_3Mn_4Si_4$ in the conventional cell, or β-$Li_{0.75}$MnSi as an alloy. We anticipated that the removal of one Li atom from β-$Li_4Mn_4P_4$ could lower E_F into the gap and produce a stable HM; it did not, however, since atoms neighboring the vacancy moved towards the vacancy, destroying the half-metallicity.

Using ABINIT, we explored the different Li concentrations of all of the studied half-Heusler alloys and found that while many were stable, none showed half-Metallic properties. The results are shown in Table V. The missing values are for calculations we stopped because the ionic relaxation process caused some of the PAW spheres to overlap by more than 25%. The PAW radii, given by the PAW data set [31], are R_C(Li) = 0.8526 Å, R_C(Mn) = 1.1176 Å, R_C(P) = 1.0091 Å,

TABLE V. Summary of lattice constants, energy differences, and magnetic moment of the half-Heusler alloys with three different Li concentrations.

Compound	Lattice constant (Å)	Total energy relative to β (eV)	Magnetic moment (μ_B/Mn)
α-$Li_1Mn_4P_4$	5.09838	0.00009	3.52314
β-$Li_1Mn_4P_4$	5.42223	0.00000	1.74490
γ-$Li_1Mn_4P_4$	5.40984	0.00033	3.18847
α-$Li_2Mn_4P_4$	5.29395	0.00027	3.84500
β-$Li_2Mn_4P_4$	5.33751	0.00000	1.13350
γ-$Li_2Mn_4P_4$	5.52909	0.00017	3.51196
α-$Li_3Mn_4P_4$			
β-$Li_3Mn_4P_4$	5.53965	0.00000	2.98656
γ-$Li_3Mn_4P_4$			
α-$Li_1Mn_4N_4$			
β-$Li_1Mn_4N_4$	4.40389	0.00000	0.29342
γ-$Li_1Mn_4N_4$			
α-$Li_2Mn_4N_4$	4.47920	0.00116	2.28075
β-$Li_2Mn_4N_4$	4.47449	0.00000	0.68456
γ-$Li_2Mn_4N_4$	4.52993	0.00105	0.00000
α-$Li_3Mn_4N_4$			
β-$Li_3Mn_4N_4$			
γ-$Li_3Mn_4N_4$			
α-$Li_1Mn_4Si_4$	5.06635	−0.00076	2.75675
β-$Li_1Mn_4Si_4$	5.54342	0.00000	2.84046
γ-$Li_1Mn_4Si_4$	5.53482	0.00010	2.79425
α-$Li_2Mn_4Si_4$			
β-$Li_2Mn_4Si_4$	5.59961	0.00000	2.84000
γ-$Li_2Mn_4Si_4$	5.61409	0.00020	2.91000
α-$Li_3Mn_4Si_4$			
β-$Li_3Mn_4Si_4$	5.69213	0.00000	3.10371
γ-$Li_3Mn_4Si_4$			

$R_C(\mathrm{N}) = 0.6350$ Å, and $R_C(\mathrm{Si}) = 1.0104$ Å. The compounds with 75% Li concentration were stable only in the β phase because Li ions are not the nearest neighbors to the TM element. The vacancy in α and γ phases is the nn to the TM element, so the unbalanced forces push the TM elements towards the vacancy and allowed the nn TMs to overlap. At 25% and 50% Li concentration, the alloys tended not to suffer from the overlap problem as much because there were two or three vacant sites for the four nn elements to occupy, respectively, resulting in less crowding. Crowding in the LiMnN alloys was more problematic due to the small size of the LiMnN cells, and $Li_3Mn_4N_4$ could not be formed in the cubic structure.

E. Stability of zinc-blende MnSi and β-LiMnSi

We carried out response-function phonon calculations on a $4 \times 4 \times 4$ irreducible $\vec{q}$ point grid for ZB MnSi at its equilibrium lattice constant and β-LiMnSi at two lattice constants: its equilibrium value and the lattice constant for which the compound is half-metallic. The results are shown in Fig. 5. MnZ in the zinc-blende structure has an unstable transverse acoustic (TA) branch along the zone boundary in the [110] direction (Γ-K). This agrees with the known fact that the ZB structure for MnP-type compounds is not the ground state of these compounds [12]. β-LiMnSi, at its equilibrium lattice constant, shows stability in the [110] direction. At the lattice constant that gives half-metallic properties, the six optical branches of β-LiMnSi are also stable. The addition of the Li atom in the structure produces a restoring force against sheer stress.

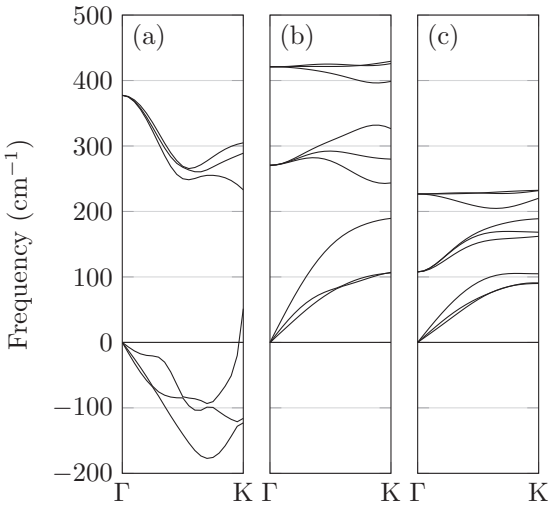

FIG. 5. The phonon bands along Γ-K of (a) zinc-blende MnSi, (b) β-LiMnSi at its equilibrium lattice constant $a = 5.778$ Å, and (c) β-LiMnSi at the lattice constant at which it is half-metallic, $a = 6.590$ Å. Negative values indicate imaginary (unstable) frequencies.

The response-function method allows for the determination of the phonon bands in the full Brillouin zone. The phonon bands for β-LiMnSi at the half-metallic lattice constant are provided in Fig. 6.

IV. SUMMARY

The fact that Li easily gives up its electron to Mn led us to investigate three Li-based half-Heusler alloys, each involving one TM element per formula, to determine the possibility of

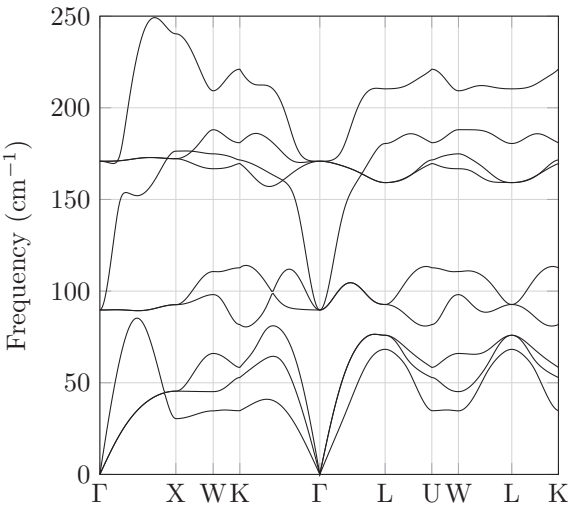

FIG. 6. The full-zone phonon bands of β-LiMnSi at a lattice constant showing half-metallic properties, $a = 6.590$ Å.

them being ferromagnetic with large magnetic moments. Three different arrangements of the atoms inside a unit cell, denoted α, β, and γ phases, appear in the literature.

We offered a unified view of bonding in the three alloys based on previous studies on TM-related half-Heusler alloys involving two TMEs [10]. The strongest bond is formed between Z and Mn, resulting in the primary bonding-antibonding gap. To understand the role played by Li, we compared the bonding properties of β-LiMnSi, a prototype, to MnSi, a HM in zinc-blende structure. Using the tetragonal cell, we found that α-LiMnP, α-LiMnN, and β-LiMnP are antiferromagnetic, while LiMnSi is a ferromagnetic HM in the β and γ phases. The reasons for the above facts were provided.

The magnetic moments for the ferromagnetic alloys are all larger than $3\mu_B$ per formula unit. At their low-strain half-metallic lattice constants, many of the alloys form large semiconducting gaps, so these alloys should be good candidates for spintronic materials for devices operating at or above room temperature due to the large gaps. A modified SP rule predicting the magnetic moments in this class of half-Heusler alloys was proposed and predicts well the three alloys with half-metallic properties; however, the rule is incapable of predicting antiferromagnetism.

The stability against shear stress, compared to the simple ZB structure, was demonstrated by calculating the phonon spectrum in the [110] direction of the Brillouin zone using the response-function scheme. We showed that MnP is unstable along the [110] direction and found that the half-metallic Li-based alloys can be stable.

Finally, we showed that the removal of Li atoms will not lower E_F into the gap region as we originally believed. Instead, the atoms surrounding the vacancy left by the Li ions will relax towards the opening and destroy the half-metallicity. Hopefully, these results will facilitate the search and subsequent growth of new HMs involving other alkalis or even alkaline metals.

ACKNOWLEDGMENTS

Work at UC Davis was supported in part by National Science Foundation Grant No. ECCS-0725902. Work at Lawrence Livermore National Laboratory was performed under the auspices of the U.S. Department of Energy by Lawrence Livermore National Laboratory under Contract No. DE-AC52-07NA27344. One of the authors (L.D.) would like to thank Dr. B. Klein for useful discussions.

[1] D. Kieven, R. Klenk, S. Naghavi, C. Felser, and T. Gruhn, I-II-V half-Heusler compounds for optoelectronics: *Ab initio* calculations, Phys. Rev. B **81**, 075208 (2010).

[2] T. Jungwirth, V. Novák, X. Marti, M. Cukr, F. Máca, A. B. Shick, J. Mašek, P. Horodyská, P. Němec, V. Holý, J. Zemek, P. Kužel, I. Němec, B. L. Gallagher, R. P. Campion, C. T. Foxon, and J. Wunderlich, Demonstration of molecular beam epitaxy and a semiconducting band structure for I-Mn-V compounds, Phys. Rev. B **83**, 035321 (2011).

[3] A. Roy, J. W. Bennett, K. M. Rabe, and D. Vanderbilt, Half-Heusler semiconductors as piezoelectrics, Phys. Rev. Lett. **109**, 037602 (2012).

[4] P. Larson, S. D. Mahanti, and M. G. Kanatzidis, Structural stability of Ni-containing half-Heusler compounds, Phys. Rev. B **62**, 12754 (2000).

[5] F. B. Mancoff, J. F. Bobo, O. E. Richter, K. Bessho, P. R. Johnson, R. Sinclair, W. D. Nix, R. White, and B. M. Clemens, Growth and characterization of epitaxial NiMnSb/PtMnSb C1 b Heusler alloy superlattices, J. Mater. Res. **14**, 1560 (1999).

[6] R. A. de Groot, F. M. Mueller, P. G. van Engen, and K. H. J. Buschow, New Class of Materials: Half-Metallic Ferromagnets, Phys. Rev. Lett. **50**, 2024 (1983).

[7] I. Galanakis, P. Mavropoulos, and P. H. Dederichs, Electronic structure and Slater–Pauling behaviour in half-metallic Heusler alloys calculated from first principles, J. Phys. D **39**, 765 (2006).

[8] J. Tobola and J. Pierre, Electronic phase diagram of the XTZ (X = Fe, Co, Ni; T = Ti, V, Zr, Nb, Mn; Z = Sn, Sb) semi-Heusler compounds, J. Alloys Compd. **296**, 243 (2000).

[9] R. W. G. Wyckoff, *Crystal Structures*, 2nd ed. (Wiley, New York, 1963), Vol. 1.

[10] M. Shauhgnessy, L. Damewood, C. Y. Fong, L. H. Yang, and C. Felser, Structural variants and the modified Slater-Pauling curve for transition-metal-based half-Heusler alloys, J. Appl. Phys. **113**, 043709 (2013).

[11] K. Schwarz, CrO_2 predicted as a half-metallic ferromagnet, J. Phys. F **16**, L211 (1986).

[12] H. Akinaga, T. Manago, and M. Shirai, Material design of half-metallic zinc-blende CrAs and the synthesis by molecular-beam epitaxy, J. Appl. Phys. **39**, L1118 (2000).

[13] J. E. Pask, L. H. Yang, C. Y. Fong, W. E. Pickett, and S. Dag, Six low-strain zinc-blende half metals: An ab initio investigation, Phys. Rev. B **67**, 224420 (2003).

[14] J. Kübler, First principle theory of metallic magnetism, Physica B+C (Amsterdam) **127**, 257 (1984).

[15] S. Baroni, S. de Gironcoli, and A. Dal Corso, Phonons and related crystal properties from density-functional perturbation theory, R. Mod. Phys. **73**, 515 (2001).

[16] G. Kresse and J. Furthmüller, Efficient iterative schemes for ab initio total-energy calculations using a plane-wave basis set, Phys. Rev. B **54**, 11169 (1996).

[17] G. Kresse and J. Furthmüller, Efficiency of *ab-initio* total energy calculations for metals and semiconductors using a plane-wave basis set, Comput. Mater. Sci. **6**, 15 (1996).

[18] G. Kresse and J. Hafner, *Ab initio* molecular-dynamics simulation of the liquid-metal–amorphous-semiconductor transition in germanium, Phys. Rev. B **49**, 14251 (1994).

[19] G. Kresse and J. Hafner, *Ab initio* molecular dynamics for liquid metals, Phys. Rev. B **47**, 558 (1993).

[20] P. Hohenberg and W. Kohn, Inhomogeneous electron gas, Phys. Rev. **136**, B864 (1964).

[21] J. P. Perdew, K. Burke, and M. Ernzerhof, Generalized gradient approximation made simple, Phys. Rev. Lett. **77**, 3865 (1996).

[22] L. Damewood and C. Y. Fong, Local field effects in half-metals: A GW study of zincblende CrAs, MnAs, and MnC, Phys. Rev. B **83**, 113102 (2011).

[23] L. Chioncel, E. Arrigoni, M. I. Katsnelson, and A. I. Lichtenstein, Electron correlations and the minority-spin band gap in half-metallic Heusler alloys, Phys. Rev. Lett. **96**, 137203 (2006).

[24] P. E. Blöchl, Projector augmented-wave method, Phys. Rev. B **50**, 17953 (1994).

[25] H. J. Monkhorst and J. D. Pack, Special points for Brillouin-zone integrations, Phys. Rev. B **13**, 5188 (1976).

[26] X. Gonze *et al.*, ABINIT: First-principles approach to material and nanosystem properties, Comput. Phys. Commun. **180**, 2582 (2009).

[27] X. Gonze, G. M. Rignanese, M. Verstraete, J. M. Beuken, Y. Pouillon, R. Caracas, F. Jollet, M. Torrent, G. Zérah, M. Mikami, P. Ghosez, M. Veithen, J. Y. Raty, V. Olevano, F. Bruneval, L. Reining, R. W. Godby, G. Onida, D. R. Hamann, and D. Allan, A brief introduction to the ABINIT software package, Z. Phys. **220**, 558 (2005).

[28] *CRC Handbook of Chemistry and Physics*, 93rd ed., edited by W. M. Haynes (CRC Press, Boca Raton, FL, 2013).

[29] C. Y. Fong, M. C. Qian, K. Liu, and L. H. Yang, Design of spintronic materials with simple structures, J. Nanosci. Nanotechnol. **8**, 3652 (2008).

[30] I. Galanakis, K. Özdoğan, and E. Şaşıoğlu, *Ab initio* electronic and magnetic properties of half-metallic NiCrSi and NiMnSi Heusler alloys: The role of defects and interfaces, J. Appl. Phys. **104**, 083916 (2008).

[31] F. Jollet, M. Torrent, and N. Holzwarth, Generation of projector augmented-wave atomic data: A 71 element validated table in the XML format, Comput. Phys. Commun. **185**, 1246 (2014).